Gas-Liquid Mass Transfer in Cocurrent Froth Flow

J. M. HEUSS, C. J. KING, and C. R. WILKE

University of California, Berkeley, California

The absorption of ammonia and oxygen in horizontal cocurrent gas-liquid froth flow in a 1-in. I.D. pipe has been investigated. At superficial liquid rates between 2 x 10^6 and 3.2 x 10^6 lb./(hr.)(sq.ft.) and superficial gas rates between 5 x 10^3 and 18 x 10^3 lb./(hr.)(sq.ft.), the length of a transfer unit in both systems was between 0.5 and 4.0 ft. The effects of distance and temperature were also investigated.

With the use of James and Silberman's data on bubble size and distribution in froth flow to estimate average bubble sizes, the gas-phase-controlled ammonia absorption data could be explained by the model of unsteady state transfer from a stagnant sphere. With the use of an interfacial-area estimate from the ammonia results, the liquid-phase-controlled oxygen absorption data were correlated by a Sherwood number characterizing the transfer from the bubbles, a Reynolds number characterizing the turbulence within the system, and the void fraction.

Gas-liquid mass transfer operations are usually carried out in equipment utilizing counter- or cross-current flow. However, cocurrent contacting of phases is just as suitable when a pure gas or liquid is employed, when an irreversible chemical reaction is taking place in the liquid phase, or, in general, when equilibrium is not closely approached between product streams. Flooding, which limits throughput in countercurrent operation, does not occur in cocurrent operation.

The general problem of multiphase flow in a pipe has been extensively studied recently. Although the ultimate goal is a knowledge of the rates of momentum, heat, and mass transfer in two-phase flow systems, the vast majority of work thus far has been concerned with momentum and heat transfer, in particular with the macroscopic properties of pressure drop, holdup, and flow pattern. The recent reviews of Dukler and Wicks (*1*) and Scott (*2*) are quite complete.

In addition to the specific applications to gas absorption, there is an added benefit to be derived from mass transfer studies. With the proper choice of mass transfer systems one can infer individual phase coefficients—something that is not possible in heat transfer studies.

The complexity of two-phase flow is dramatically brought out by the variety of possible flow patterns. The most useful chart for predicting flow patterns in horizontal flow is that of Baker (3), shown in Figure 1. It is a plot of gas mass velocity G [lb./(hr.)(sq.ft.)] as a function of the ratio of liquid to gas mass velocities L/G, with empirical correction factors for variations in physical properties. The lines dividing the flow patterns are actually broad transitions.

The highest interfacial areas and highest transfer rates should occur in the froth-flow regime, which is characterized by high throughputs and by a high level of turbulence in the continuous phase. This study was concerned with mass transfer in horizontal cocurrent gas-liquid froth flow in a pipe.

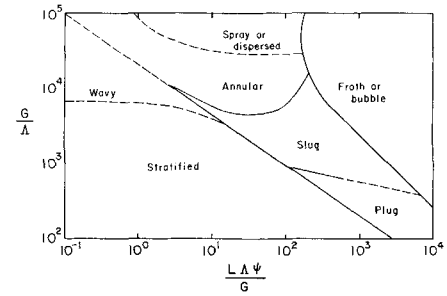

Figure 1. Baker correlation of flow patterns in gas-liquid horizontal flow.

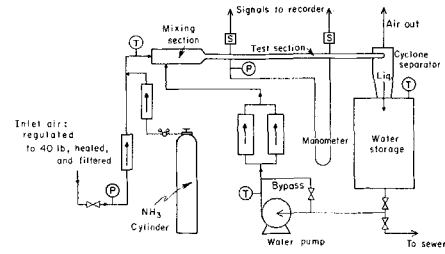

Fig. 2. Schematic drawings of gas-liquid contacting apparatus. *P*, pressure gauge. *T*, thermometer. *S*, sampling tap and measuring cell. ↑, rotameter.

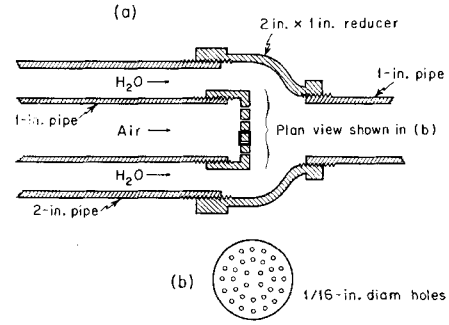

Fig. 3. Mixing section. *(a)* Cross section. *(b)* Plan view.

J. M. Heuss is with General Motors Research Laboratories, Warren, Michigan.

EQUIPMENT

The equipment is shown schematically in Figure 2. Air and distilled water were brought together in a mixing section to form a froth, which passed through a 1-in. I.D. Lucite test section into an aluminum cyclone separator. The liquid fraction from the separator was returned to a liquid storage tank for recirculation, while the gas fraction passed out to the atmosphere. The liquid was pumped from a 55-gal. steel storage drum and metered into the mixing section. The air, supplied by a 100-lb./sq. in. gauge dry air line, was reduced by a regulator system, heated, filtered, metered, and delivered to the mixing section. The mixing section, shown in Figure 3, was made from standard galvanized pipe. The 4-ft.-long Lucite test section had pressure and sampling taps drilled and tapped (⅛-in. N.P.T.) so that measurements could be made over 6-in., 1-ft., and 2-ft. distances.

For oxygen absorption liquid samples were drained from the test section and metered through polarographic oxygen cells. For ammonia absorption liquid samples were drained from the test section and metered through electrical conductivity cells. A detailed description of the equipment, the sampling and measuring devices in particular, is given elsewhere (*4*).

PROCEDURE

Oxygen Absorption

The liquid returning to the storage tank from the separator was in equilibrium with air at 1 atm. and the temperature of the run, as confirmed by the Winkler titration. Since the temperature remained constant during a run, the concentration of oxygen in the liquid entering the test section was constant.

Each oxygen run consisted of two parts. First, with only water flowing in the test section, valves on the sampling rotameters were opened, allowing water to pass through two polarographic cells at a constant rate (1 to 2 cc./min.). The water became aerated through mass transfer in the separator. The signals from the cells were recorded after they came to steady state, giving the oxygen concentration in water in equilibrium with air at 1 atm. and the temperature of the run. Second, with the two-phase mixture flowing, the sampling valves were opened and the flow rate of water through the polarographic cells was adjusted to be equal to that used in the first part of the run. This was a small enough flow, so that no bubbles were entrained into the cells or into any part of the sample line. The entire sample line was transparent, so that any bubbles could be observed. The liquid was contacted with air at a pressure above atmospheric in the test section and therefore it absorbed air, the equilibrium concentration at any point being determined by the pressure. The cell readings were recorded after 10 to 15 min. at steady state. If any air was seen in the transparent cell housing, the readings were disregarded and the run terminated.

Ammonia Absorption

In the ammonia system, three sampling taps and three conductivity cells were used: one for the liquid entering the test section and two in the test section. With the froth flowing, valves on the three sampling lines were opened and liquid samples were metered at 2 cc./min. through each line. The ammonia regulator was opened and anhydrous ammonia was metered into the gas stream to give about 2% ammonia entering the mixing section. The system absorbed for 2 min. and then the Hoke valves above and below each conductivity cell were simultaneously shut off, capturing three samples. The samples represented conditions within a 2- or 3-sec. period, during which the bulk concentration changed at most 3%.

EXPERIMENTAL PROGRAM

A series of preliminary experiments was carried out to insure that the flow within the test section was fully developed. These included visual observations, high-speed photography, and pressure-drop measurements. A number of simple mixing sections were tried. The final configuration (shown in Figure 3) provided for the formation of bubbles and their mixing with the liquid stream. It also provided the most stable operation (least slugging) and developed the energy dissipation rates in a short distance.

A series of experiments was then carried out to investigate the effects of liquid rate, gas rate, temperature, and distance on the absorption of ammonia and oxygen from air into water.

TREATMENT OF DATA

For the two absorption systems under consideration, the bulk molar flow rates do not change significantly. Hence the following equations apply:

$$l = \frac{-G_M}{K_G a P} \int_{p_1}^{p_2} \frac{dp}{p - p_e} \tag{1}$$

$$l = \frac{L_M}{K_L a \rho_M} \int_{c_1}^{c_2} \frac{dc}{c_e - c} \tag{2}$$

The integrals are the number of transfer units (NTU).

$$(NTU)_{OG} = \int_{p_2}^{p_1} \frac{dp}{p - p_e} \tag{3}$$

$$(NTU)_{OL} = \int_{c_1}^{c_2} \frac{dc}{c_e - c} \tag{4}$$

The length of a transfer unit (LTU) is then

$$(LTU)_{OG} = \frac{G_M}{K_G a P} \tag{5}$$

$$(LTU)_{OL} = \frac{L_M}{K_L a \rho_M} \tag{6}$$

Following the classical addition-of-resistances concept, the overall coefficients may be related to individual phase coefficients.

$$(LTU)_{OG} = (LTU)_G + (mG_M/L_M)(LTU)_L \tag{7}$$

$$(LTU)_{OL} = (LTU)_L + (L_M/mG_M)(LTU)_G \tag{8}$$

where $(LTU)_G$ and $(LTU)_L$ are defined as

$$(LTU)_G = G_M/k_G a P \tag{9}$$

$$(LTU)_L = L_M/\rho_M k_L a \tag{10}$$

$k_L a$ and $k_G a$ are the coefficients defined on the basis of interfacial concentrations.

At the liquid and gas rates used, $(mG_M/L_M)(LTU)_L$ for ammonia was always less than 0.005 $(LTU)_G$ so that $(LTU)_{OG} \approx (LTU)_G$ and the transfer was almost completely gas-phase controlled. Similarly, $(L_M/mG_M)(LTU)_G$ for oxygen absorption was always less than 0.02 $(LTU)_L$, so that $(LTU)_{OL} \approx (LTU)_L$ and this case was almost completely liquid-phase controlled.

In reality the classical additivity-of-resistances concept may not hold exactly because of the relatively wide range of bubble sizes to be expected. However, the conclusions regarding gas- and liquid-phase control for the oxygen and ammonia systems should still be valid (*5*).

This analysis also assumes negligible axial mixing and complete radial mixing. The axial mixing assumption is warranted by the very high velocities of flow, while the radial mixing assumption is favored by the visibly high degree of agitation of the flow. It is possible that more refined sampling techniques could yield some modification of the results. Sampling in systems of this kind is deserving of further study.

Ammonia

The high ratio of liquid to gas rates kept p_e always less than 1% of p. Therefore Equation (3) integrates to

$$(NTU)_{OG} \approx \ln p_1/p_2 \qquad (11)$$

This analysis assumes constant G_M and constant P. As ammonia is being absorbed water is being vaporized, so that G_M is slightly changed. In the measurement section P changes about 5%, while p changes by a factor of 2 or more. These effects were taken into consideration and small corrections applied. They changed $(NTU)_{OG}$ by about 5%, which was approximately the precision of the conductivity measurements. The cooling effect of vaporization was offset by heating in the pump so that the temperature remained nearly constant during a run.

Oxygen

In the oxygen case, water saturated with air at 1 atm. was contacted with air at higher pressures, the temperature remaining constant. Since Henry's law constant of oxygen is independent of pressure up to about 10 atm., the equilibrium concentration of oxygen is given by

$$c_e = y_{O_2}(P - p_w)/H \qquad (12)$$

Schmidt numbers of water and ammonia in air are about equal. Therefore mass transfer coefficients from the ammonia results were used to calculate p_w at any point.

The total pressure was decreasing down the test section; hence the equilibrium concentration of oxygen in water was decreasing. The effect was such as to make c_e more nearly linear in distance along the pipe rather than linear in c. This factor was taken into account in the integration of Equation (4), and the resultant values of $(NTU)_{OL}$ were different by about 10% from those that would have been computed by an integration of Equation (4) assuming c_e linear in c. More details on this calculational procedure are given elsewhere (*4*).

RESULTS AND DISCUSSION

Visual Studies

The mixing section always formed a froth. At flow rates below those of froth flow the froth broke up as it passed down the test section into that flow pattern that was stable at the given conditions. As froth flow was approached from the slug flow region, fewer and fewer slugs were observable until the flow appeared to be homogeneous throughout the test section.

High-speed photographs were taken using a General Radio Strobotac. Slug flow appears to be a mass of small bubbles with many large slugs of gas, whereas froth or bubble flow appears to be a homogeneous mass of small bubbles. It is somewhat arbitrary where one defines the transition between these flow regimes, since there are always a few slugs present in froth flow. Nevertheless, the area Baker calls froth or bubble flow satisfies a visual definition.

Pressure Drop

An extensive series of pressure drop measurements was carried out over flow sections of different lengths. Over the range of flow conditions employed for the mass transfer studies, the pressure drop varied from 0.3 to 1.5 lb./(sq. in.)(ft.). Pressure drop data taken over sections of varying length following the entry section (after Section E in Figure 4) indicated that dP/dl became constant after that point. This observation suggests that stable flow was rapidly established.

These data were analyzed by means of an adaptation of the Bankoff variable density homogeneous flow model (*6*), using the Hughmark correlation (*7*) for estimation of the local void fraction. The Bankoff model assumes radial variations in the void fraction, which give rise to

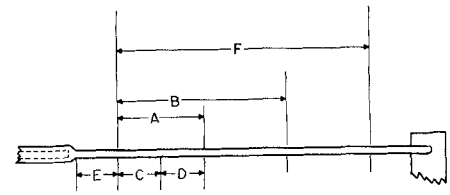

Fig. 4. Measurement sections. *A*, 1-ft. test section. *B*, 2-ft test section. *C*, 6-in. test section. *D*, 6-in. test section. *E*, 6-in. entrance section. *F*, 3-ft test section.

an apparent slip of the phases on a macroscopic scale even though there is no slip on a microscopic scale. Bankoff takes the mean velocity for use in the model to be

$$U_m = U_{TP} = \frac{L}{\rho_L} + \frac{G}{\rho_G} = U_{LS} + U_{GS} \qquad (13)$$

A better prediction of the pressure drop data of the present study was obtained using a *homogeneous* mixture velocity defined as

$$U_m = U_{hom} = \frac{L + G}{\rho_m} \qquad (14)$$

where

$$\rho_m = \rho_L(1 - \alpha) + \rho_G\alpha \qquad (15)$$

U_{hom} also provides a better correlation than U_{TP} for the pressure drop data of Johnson and Abou-Sabe (*8*) and Martin (*9*). In cases where there is an apparent slip on a macroscopic basis and the superficial velocities of gas and liquid are not equal, U_{hom} is more closely related to the superficial velocity of the liquid phase, which carries the bulk of the kinetic energy of the flow. A detailed pressure drop analysis is given elsewhere (*4*).

Ammonia Absorption

Liquid and Gas Rates. The absorption of ammonia over the 1-ft. section marked A on Figure 4 was measured in a set of twelve runs at four gas rates [from 5,250 to 12,000 lb./(hr.)(sq.ft.)] and three liquid rates [from 2,060,000 to 2,980,000 lb./(hr.)(sq.ft.)]. A least-squares regression analysis by digital computer fits the data to the form

$$(LTU)_G = \frac{a}{L^b G^c} \qquad (16)$$

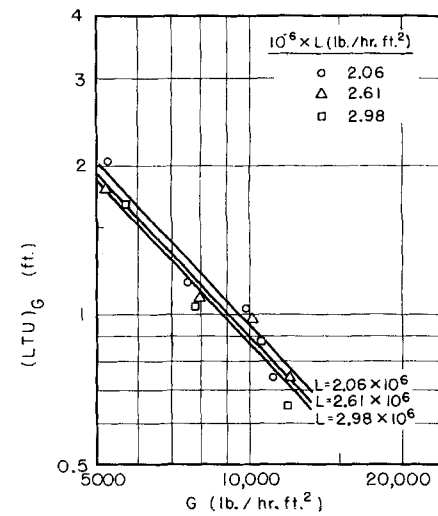

Figure 5. Experimental results for ammonia absorption. Gas phase resistance to mass transfer.

with the result

$$(LTU)_G = \frac{9.0 \times 10^5}{L^{0.25} G^{1.1}} \tag{17}$$

The results are shown in Figure 5, along with a series of lines representing Equation (17). A complete tabulation of run conditions is available elsewhere (*4*).

$k_G a$. Values of the individual phase mass transfer coefficient $k_G a$ were calculated from

$$k_G a = \frac{G_M}{P_{av}\, l} (NTU)_G \tag{18}$$

The volumetric coefficient $k_G a$ is the product of an individual phase coefficient and the interfacial area per unit volume. If one can break out a from the volumetric coefficient, one can gain greater insight into the individual phase coefficients k_G and k_L.

For a system of many spherical particles consisting of N_i particles of diameter d_i in a given size interval dispersed in a medium, the mean surface-volume diameter is defined as

$$d_{sv} = \frac{\sum_i N_i d_i^3}{\sum_i N_i d_i^2} \tag{19}$$

where the summation is over all size intervals. For a volume fraction of dispersed phase α, the interfacial area per unit volume is given by

$$a = \frac{6\alpha}{d_{sv}} \tag{20}$$

The simplest model one can assume for gas-phase mass transfer is that of unsteady state transfer to a stagnant sphere with negligible external resistance. This problem has been solved for a single bubble, resulting in a series solution

$$Y = \frac{p_o - p_f}{p_o - p_e} = 1 - \frac{6}{\pi^2} \sum_{n=1}^{\infty} \frac{1}{n^2} \exp\left(-\frac{4D n^2 \pi^2 t}{d^2}\right) \tag{21}$$

for the case where p_e is constant.

Vermeulen (*10*) has shown that the solution can be approximated by

$$Y = 1 - e^{-\frac{4D\pi^2 t}{d^2}} \tag{22}$$

for $Y > 0.4$. From the definition of $k_G a$ in a gas-phase controlled system we find that Equation (22) leads to

$$k_G a = \frac{4D\pi^2}{RTd^2} \tag{23}$$

and

$$(NTU)_G = \frac{4D\pi^2 t}{d^2} \tag{24}$$

Equations (23) and (24) apply to a single bubble of diameter d. In extending these equations to the flow situation of the present study one must allow for the voidage and must employ an average diameter characterizing the distribution of bubble sizes.

$$k_G a = \frac{4\alpha D\pi^2}{RT\, d_{av}^2} \tag{25}$$

$$(NTU)_G = \frac{4\alpha D\pi^2 t}{d_{av}^2} \tag{26}$$

The average degree of equilibration of the entire gas phase for any contact time t is given by a volumetric average over all bubbles.

$$Y_{av} = \frac{\sum_i Y_i V_i}{\sum_i V_i} = \frac{\sum_i Y_i N_i d_i^3}{\sum_i N_i d_i^3} \tag{27}$$

If $Y_{av} > 0.4$, then by Equation (22)

$$Y_i = 1 - e^{-\frac{4D\pi^2 t}{d_i^2}} \tag{28}$$

and

$$Y_{av} = 1 - e^{-\frac{4D\pi^2 t}{d_{av}^2}} \tag{29}$$

If the distribution of bubble size is known, Y_{av} and d_{av} may be calculated from Equations (27), (28), and (29) for a given contact time.

Such a calculation of d_{av} reflects two effects of the bubble size distribution. The first is a driving force effect. The smallest bubbles equilibrate faster, contributing less and less to the transfer as time goes on because of a lesser driving force. This acts to raise d_{av} after appreciable equilibration has occurred. Secondly, under conditions of uniform driving force, an average or effective k_G is based on the area over which transfer is taking place.

$$k_{G_{av}} = \frac{\sum_i k_{Gi} A_i}{\sum_i A_i} \tag{30}$$

If the definition of a is substituted in Equation (23), it can be seen that k_G is itself inversely proportional to d and

$$k_{G_{av}} \sim \frac{\sum_i \frac{1}{d_i} N_i d_i^2}{\sum N_i d_i^2} = \frac{\sum_i N_i d_i}{\sum N_i d_i^2} \tag{31}$$

which introduces a "diameter-surface" mean diameter

$$d_{ds} = \frac{\sum_i N_i d_i^2}{\sum_i N_i d_i} \tag{32}$$

From Equations (20) and (31) it follows that if there is a uniform driving force for all bubbles with a given contact time

$$k_G a = \frac{4\alpha D\pi^2}{RT\, d_{sv}\, d_{ds}} \tag{33}$$

James and Silberman (*11*) report data on bubble size and distribution in froth flow at low void fractions obtained photographically. Values of d_{ds}, d_{sv}, and d_{av} were computed for several of the James and Silberman distributions and the conditions of the present ammonia absorption runs. From Equation (19) d_{sv} is equivalent to a diameter exceeded by 5 to 10% of the bubbles (number basis); from Equation (32) d_{ds} is equivalent to a diameter exceeded by 15 to 20% of the bubbles. For small contact times ($Y_{av} < 0.2$), d_{av} from Equations (27), (28), and (29) is equivalent to a diameter exceeded by about 10% of the bubbles as would be expected if d_{av}^2 were the product $d_{sv} d_{ds}$ as in Equation (33). This follows since the driving force is relatively uniform at $Y_{av} < 0.2$. As Y_{av} increases d_{av} increases because of the driving force effect so that at Y_{av} between 0.4 and 0.9 (the conditions of the present ammonia runs), d_{av} is equivalent to a diameter exceeded by 4 to 6% of the bubbles. Thus d_{av} is taken to be equivalent to d_{95} (the diameter exceeded by 5% of the bubbles). Figure 6 shows d_{50}, the diameter exceeded by 50% of the bubbles, and d_{95} as a function of

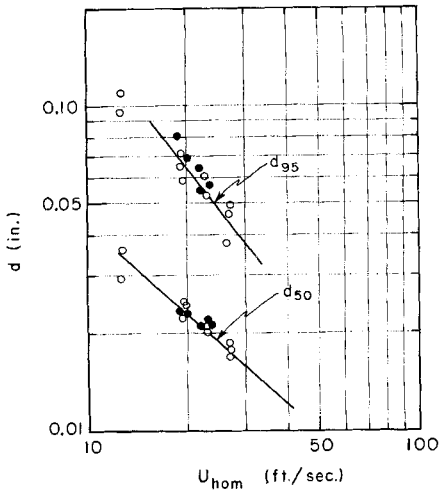

Fig. 6. Bubble diameter vs. U_{hom}. Data of James and Silberman. Solid 4-in. diam. pipe. Open 2½-in. diam. pipe.

U_{hom}. The separation of the two lines affords an indication of the width of the size distributions. The two points with U_{hom} less than 15 ft./sec. are in the transition region between slug and froth flows. These two distributions differ from those at higher U_{hom} by having considerably more large bubbles. If these two points are excluded it can be seen that d_{50} varies as U_{hom}^{-1} and d_{95} varies as $U_{hom}^{-1.5}$; hence one may conclude that d_{av} varies as $U_{hom}^{-1.5}$.

Measurements of high-speed photographs showed that d_{50} near the wall in the present system was in the range of 0.01 to 0.03 in., in general agreement with James and Silberman at equivalent values of U_{hom}. However, there may be a significant wall effect. As Kolmogoroff predicted (*12*) and Sleicher (*13*) found, drops in a liquid-liquid system of low void fraction break up sooner near the wall. James and Silberman do not mention a wall effect in their air-water system.

There may also be an effect of void fraction on bubble diameter. Calderbank (*14*) measured interfacial areas in gas-liquid mixtures in agitated tanks in which gas was being sparged through the liquid, and found d_{sv} proportional to $\alpha^{1/2}$ for a case of considerable relative velocity between phases. Vermeulen, Williams, and Langlois (*15*) measured interfacial areas in gas-liquid mixtures in closed agitated tanks with less relative velocity between phases. From their work one might expect an increase in bubble size of about a factor of 2 between void fractions of 0.05 and 0.50.

From the James and Silberman data one can estimate that d_{av} would range from about 0.04 to 0.09 in. at low void fractions ($\alpha < 0.1$) and at the velocities encountered in the present work. Allowing for a factor of from 1.5 to 2.5 increase in diameter coming from the higher voidages (0.4 to 0.7) in the present work, and for smaller increases due to a wall effect and/or a small amount of undetectable slugging, it seems reasonable to assign a value of d_{av} on the order of 0.06 to 0.27 in. to the flow conditions involved in the ammonia data. Any higher estimate would not be consistent with the photographic determination of d_{50}.

Since Y was always greater than 0.4 in the 1-ft. measuring section A, one can apply Equations (22), (23), and (25) to the results. Substituting $D_{NH_3} = 0.78$ sq.ft./hr. and values of k_Ga and α into Equation (25), a calculation shows d_{av} to vary from 0.12 to 0.27 in., in agreement with the previous estimation of 0.06 to 0.27 in. based on the James and Silberman data. Any turbulence, circulation, breakup, oscillation, or distortion would increase the transfer. The conclusion therefore is that the bubbles are acting largely as rigid spheres, the high molecular diffusivity overriding any breakup or turbulence that might be occurring. This conclusion is consistent with the assumption of no microscopic slip used in predicting pressure gradients. Small bubbles flowing along with a turbulent liquid would be expected to act as rigid spheres if there is no relative velocity.

A least-squares regression analysis fit k_Ga as

$$k_Ga = 0.016\,\alpha^{2 \pm 0.3}\,U_{hom}^{3.2 \pm 0.2} \qquad (34)$$

where α is obtained from the Hughmark correlation (7). If k_Ga varies inversely with the diameter squared and the bubble diameter is a function of U_{hom} within the system

$$d_{av} \sim U_{hom}^{-1.6 \pm 0.1} \qquad (35)$$

This agrees with the dependence of James' and Silberman's d_{95} on $U_{hom}^{-1.5}$, and the finding of Vermeulen, Williams, and Langlois (*15*) that d_{sv} in gas-liquid mixtures in agitated tanks varies as impeller velocity to the — 1.5 power.

Equation (25) predicts a dependence of k_Ga on α to the first power as opposed to the dependence to the second power shown in Equation (34). As mentioned earlier, any dependence of d_{sv} on α should be positive, which would tend to decrease the dependence of k_Ga on α. The power on α may therefore be anomalous or it may be possible that k_G is a positive function of α due to breakup and deformation at the higher void fractions where something similar to close packing is approached. A larger percentage of bubbles breaking up and reforming would increase k_Ga.

Distance. In the initial period ($Y < 0.4$), the unsteady state diffusion model predicts a higher value of k_Ga. Indeed values of k_Ga measured over the 6-in. entrance section E were about twice as large as those measured over the next 1-ft. section, A, where Y was always greater than 0.4. This is in qualitative agreement with Equation (21). The length of a transfer unit increased down the test section changing most rapidly at first and approaching a constant value in sections A and C. Equilibrium was approached too fast to measure the transfer over more than a 1-ft. section.

Temperature. The effect of temperature was assessed in three runs made at fixed-weight flow rates of gas and liquid over a range of 18° to 28°C. The results are fit by

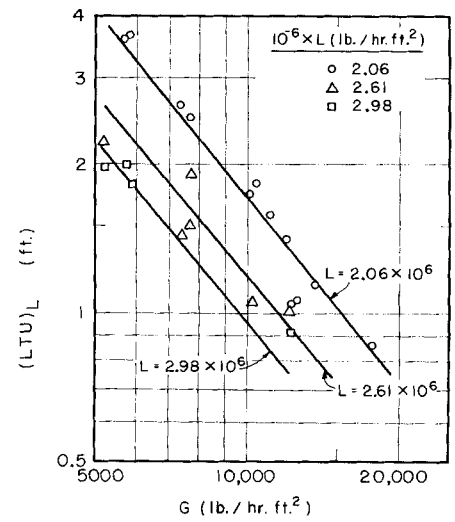

Fig. 7. Experimental results for oxygen absorption. Liquid phase resistance to mass transfer.

$$k_G a \sim e^{(-0.010 \pm 0.002)T} \quad (36)$$

where T is in °K.

An attempt to check whether the temperature dependence of Equation (25) is consistent with the measured temperature dependence of $k_G a$ was inconclusive because of lack of knowledge concerning the effects of temperature on d_{av} and α.

Oxygen Absorption

Liquid and Gas Rates. The absorption of oxygen was measured over the 1-ft. section A in Figure 4 in a set of twenty-eight runs at gas rates from 5,150 to 17,600 lb./(hr.)(sq.ft.) and liquid rates from 2×10^6 to 3.2×10^6 lb./(hr.)(sq.ft.). The results, corrected for gas-phase resistance using Equation (8), are presented in Figure 7; a more complete tabulation of experimental conditions is available elsewhere (*4*). The correction was never more than 2%.

A least-squares regression analysis fit the data as

$$(LTU)_L = 3.8 \times 10^{15} \ (L)^{-1.65} \ (G)^{-1.28} \quad (37)$$

The lines drawn in Figure 6 represent the predictions of Equation (37) for three different liquid flow rates. The individual datum points were corrected by $L^{-1.65}$ to the nearest of the three liquid flow rates considered in Figure 6.

$k_L a$. Values of $k_L a$ were calculated from

$$k_L a = \frac{L_M (NTU)_L}{\rho_M \, l} \quad (38)$$

Dimensional analysis leads to

$$N_{Sh} = f(N_{Re}, N_{Sc}, \alpha) \quad (39)$$

A least-squares regression analysis fit $k_L a$ as

$$k_L a = (\text{const.}) \ U_{hom}{}^{4.1 \pm 0.25} \ \alpha^{-2.0 \pm 0.25} \quad (40)$$

Using the estimate of d_{sv} from the ammonia results, a was removed from $k_L a$ by means of Equation (20). d_{sv} was taken equal to d_{av} computed for the ammonia results by Equations (25) and (34), since both are nearly equal to d_{65}. Taking d_{ds} as 0.80 times d_{sv}, Equation (40) is rearranged into dimensionless form as

$$\left(\frac{k_L \, d_{ds}}{D_L}\right) = 0.0316 \left(\frac{2R_P \, U_{hom} \, \rho_L}{\mu_L}\right)^{0.9} \left(\frac{1}{\alpha}\right)^3 \quad (41)$$

where $\dfrac{k_L d_{ds}}{D_L}$ is a Sherwood number and $2R_P U_{hom} \rho_L / \mu_L$ is a Reynolds number.

The Sherwood group should also be a function of the Schmidt group; however, there was no direct means of ascertaining this dependency in this study. The temperature dependency of $k_L a$ was measured (see below), but there is again no reliable way to estimate the effect of temperature on α and d_{ds} in Equation (41).

The Reynolds number in Equation (41) is based on the pipe diameter, while the Sherwood number is based on the bubble diameter. Previous work involving mass transfer to and from spheres has generally been concerned either with conditions of significant relative velocity between the phases where correlation was in terms of a Reynolds number based on that relative velocity, or with conditions of practically no relative velocity, which are analogous to those of a stationary particle suspended in an infinite stagnant fluid. In the latter case

$$\frac{k_L \, d}{D} = 2 + \frac{d}{\sqrt{\pi D t}} \quad (42)$$

for a single bubble (*16*), and

$$\frac{k_L \, d_{ds}}{D} = 2 + \frac{d_{ds}}{\sqrt{\pi D t}} \quad (43)$$

for a distribution of bubbles, where t is time following first contact of the bubble with the liquid.

An equation of the same general form as Equation (43) would be expected for the conditions of the present study if liquid-phase transport occurred solely through molecular diffusion, although some correction would be required since the medium surrounding a given bubble is not infinite. Application of the equation would also require that none of the gas bubbles change composition appreciably. This assumption is substantiated by a calculation.

The pressure drop and ammonia absorption results were amenable to treatment assuming no relative velocity on the microscopic scale. If it is assumed that there is no relative velocity, Equation (43) would apply in an infinite turbulent fluid, provided D was replaced by a constant transport coefficient that would properly describe the enhancement of the diffusion process provided by the turbulence. Present knowledge of the turbulent characteristics of two-phase flow is so limited that it makes prediction of such an effective transport coefficient extremely difficult.

The calculated Sherwood numbers are very large (6,000 to 20,000); the rate of oxygen absorption was from 10 to 100 times larger than predicted by Equation (43) using the molecular diffusivity. This high turbulence level should cause steady state to be reached very fast. At steady state the first term on the right side of Equation (43) predominates over the transient term and k_L is inversely proportional to d_{ds}. Constancy of $k_L a$ in the region of measurement was confirmed by comparing oxygen data obtained over Sections A and B of Figure 4. Thus the form of the Sherwood group is indicated as $k_L d_{ds}/D$.

A Reynolds number based on the pipe diameter would be expected to characterize the turbulence level of the flowing continuous liquid phase. The 0.9 power on the Reynolds number is similar to that found in heat and mass transfer in forced convection near fixed interfaces.

The void fraction appears in Equation (43) to the minus third power. A possible explanation of the negative power on α may be offered in terms of a damping effect on the turbulence. Hinze (*17*) pointed out that interactions between particles become important as the concentration of particles is increased in a suspension of solids. Indeed as the maximum packing of particles is approached a severe damping of the turbulence is expected. Bagnold (*18*), working with solid particles, noted a freezing of turbulence as he approached close packing. If the bubbles in the present work are assumed to be rigid spheres, close packing would be approached in the range of void fractions between 0.4 and 0.7.

Temperature. The effect of temperature on $k_L a$ was determined in a series of four runs at fixed-weight flow conditions of gas and liquid over the range of 19° to 34°C. The results are fit by

$$k_L a \sim e^{(0.042 \pm 0.008)T} \quad (44)$$

where T is in °K.

CONCLUSIONS

High-speed photographs of the flow near the wall suggest that froth flow is a homogeneous mixture of small bubbles. Bankoff's variable-density homogeneous flow model (*6*) can be combined with the Hughmark correlation for void fraction and the homogeneous velocity (U_{hom}) to predict pressure gradients in froth flow. The homogeneous mixture velocity can be used as a parameter

to characterize the energy dissipation per unit mass and time.

The ammonia absorption data are gas-phase controlled and can be explained by using the simple model of transfer from a stagnant sphere. Average bubble sizes calculated from the mass transfer data using this model are in agreement with a prediction made from the data of James and Silberman (*11*), the only data available on bubble size and distribution in froth flow. The bubbles act as rigid spheres with no relative velocity between phases with the possible exception of an effect of breakup at high void fractions.

By using the estimate of interfacial area deduced from the ammonia results to break out k_L from k_La, the liquid-phase controlled oxygen absorption data may be correlated by a Sherwood number characterizing the transfer from the bubbles and a Reynolds number characterizing the turbulence within the system. A negative dependence on void fraction is explained as an effect of damping of the turbulence.

The length of a transfer unit in both systems lies in the range of 0.5 to 4 ft. At the high velocities employed equilibrium is approached within 0.1 sec. The combination of a high interfacial area and a high turbulence level explain the rapid transfer.

The transfer rate increases faster than the throughput so that the length of a transfer unit *decreases* as the residence time decreases. The rate coefficient k_L or k_G is dependent on the bubble size. As the turbulence level is increased, k_L is increased. The average bubble size is also decreased, which serves to increase both the interfacial area and k_G and also serves to increase k_L further.

ACKNOWLEDGMENT

This work was carried out in the Lawrence Radiation Laboratory under the auspices of the U.S. Atomic Energy Commission.

NOTATION

a = interfacial area per unit pipe volume, ft.$^{-1}$
c = solute concentration in liquid, moles/vol.
c_e = solute concentration in liquid in equilibrium with gas, moles/vol.
D = diffusivity, sq.ft./hr.
d = bubble diameter, in.
G = superficial mass velocity of air, lb./(hr.)(sq.ft.)
g_c = gravitational constant, lb.$_m$-ft./lb.$_f$-sec.^{2}
H = Henry's law constant, atm.-vol./lb.-mole
k_G = individual gas-phase coefficient, lb-mole/(hr.)(sq.ft.) atm.
k_L = individual liquid-phase coefficient, lb.-mole/(hr.)(sq.ft.) unit Δc
K_Ga = overall gas-phase coefficient on a volume basis, lb.-moles/(hr.)(cu.ft.) atm.
K_La = overall liquid-phase coefficient on a volume basis, lb.-moles/(hr.)(cu.ft.) unit Δc
k_Ga = gas-phase coefficient on a volume basis, lb-moles/(hr.)(cu.ft.)(atm.)
k_La = liquid-phase coefficient on a volume basis, lb-moles/(hr.)(cu.ft.) unit Δc
L = superficial mass velocity of liquid, lb./(hr.)(sq. ft.)
l = length of test section, ft.
LTU = length of a transfer unit, ft.
m = dy_e/dx = slope of equilibrium curve, dimensionless
N_{Se} = Reynolds number, dimensionless
N_{Re} = Schmidt number, dimensionless
N_{Sh} = Sherwood number, dimensionless
N_i = number of bubbles with diameter d_i in unit volume
NTU = number of transfer units, dimensionless
P = total pressure, atm.
p = partial pressure of solute, atm.
p_e = partial pressure of solute in equilibrium with liquid, atm.
R = gas constant, cu.ft.-atm./(lb.-mole) (°R.)
R_P = radius of pipe, ft.
T = temperature, °C. or °K.
t = time, sec.
U = velocity, ft./sec.
Y = equilibration level of bubble, dimensionless
y = mole fraction of solute in gas, water free basis, dimensionless

Greek Letters

α = in situ void fraction, dimensionless
Λ = density parameter = $[(\rho_G/0.075)(62.3/\rho_L)]^{1/2}$
μ = viscosity, centipoises
ρ = density, lb./cu.ft.
σ = surface tension, dynes/cm.
ψ = viscosity and surface tension parameter = $\frac{73}{\sigma}\left[\mu_L\left(\frac{62.3}{\rho_L}\right)^2\right]^{1/3}$

Superscripts

b, c = exponents to be determined, Equation (16)

Subscripts

av = average
ds = mean, surface diameter
f = final
G = gas
GS = superficial gas
hom = homogeneous
L = liquid
LS = superficial liquid
M = on a molar basis
m = two-phase mixture; for density, $\rho_m = \rho_L(1 - \alpha) + \rho_G\alpha$
o = initial
OG = overall gas
OL = overall liquid
sv = mean, surface-volume
TP = two-phase mixture, averaged over cross section
w = water vapor
1 = start of measuring section
2 = end of measuring section
50 = exceeded by 50%
95 = exceeded by 5%

LITERATURE CITED

1. Dukler, A. E., and M. Wicks, in "Modern Chemical Engineering," Vol. 1, p. 349, Reinhold, New York (1963).
2. Scott, D. S., *Advan. Chem. Eng.*, **4**, 200 (1964).
3. Baker, O., *Oil Gas J.* (June 26, 1954).
4. Heuss, J. M., C. J. King, and C. R. Wilke, "Mass Transfer in Cocurrent Gas-Liquid Flow," *U.S.A.E.C. Rept. UCRL-11570*, Lawrence Radiation Laboratory, Berkeley, California (1964).
5. King, C. J., *A.I.Ch.E. J.*, **10**, 671 (1964).
6. Bankoff, S. G., *Trans. Am. Soc. Mech Engrs.*, **82**, 265 (1960).
7. Hughmark, G. A., *Chem. Eng. Progr.*, **58**, 62 (1962).
8. Johnson, H. A., and A. H. Abou-Sabe, *Trans. Am. Soc. Mech. Engrs.*, **74**, 977 (1952).
9. Martin, F. W., M.S. thesis, Univ. California, Berkeley (1963).
10. Vermeulen, T., *Ind. Eng. Chem.*, **45**, 1664 (1953).
11. James, W., and E. Silberman, *Univ. Minnesota Tech. Paper No. 26, Ser. B* (1956).

12. Kolmogoroff, A. N., *Dokl. Akad. Nauk SSSR*, **66**, 825 (1949).
13. Sleicher, C. A., *A.I.Ch.E. J.*, **8**, 471 (1961).
14. Calderbank, P. H., *Trans. Inst. Chem. Engrs.*, **36**, 443 (1958).
15. Vermeulen, T., G. M. Williams, and G. E. Langlois, *Chem. Eng. Progr.*, **51**, 85F (1955).
16. Epstein, P. S., and M. S. Plesset, *J. Chem. Phys.*, **18**, 1505 (1950).
17. Hinze, J. O., "Turbulence," McGraw-Hill, New York (1959).
18. Bagnold, R. A., *Phil. Trans. Roy. Soc. (London)*, **249**, 235 (1956); *Proc. Roy. Soc.*, **A225**, 49 (1954).

Manuscript received November 2, 1964; revision received April 28, 1965; paper accepted April 30, 1965.

Effects of Mixing on Chain Reactions in Isothermal Photoreactors

FRANK B. HILL and RICHARD M. FELDER

Brookhaven National Laboratory, Upton, New York

An analytical study of the interaction of mixing, radiation attenuation, and chemical kinetics in isothermal photoreactors is presented. For a particular chain reaction mechanism in the presence of stationary state kinetics and low conversion, the conditions required for the existence of mixing effects are formally stated, and the direction of change of conversion and quantum yield resulting from the introduction of mixing is established. Calculated results are presented for monoenergetic, unidirectional sources. Factors considered include mode of chain termination, radiation attenuation law, photoreactor geometry, state of mixing, and reactor optical thickness. Chemical and mixing time scale considerations are discussed.

Much attention has been given in recent years to the effects of mixing on chemical reactor performance. Most of the work done has involved simple, single-step thermal reactions. Very little has been done on mixing as it affects the performance of photoreactors, especially in the presence of typical complex reactions of industrial interest.

Many sources exist that suggest that mixing may under certain circumstances be beneficial to photoreactor performance (*1* to *5*). While it is not always clear what the precise cause of improved performance is, the introduction of turbulence seems to be a factor in all cases, the turbulence arising from high flow rates, stirring or agitation, or the use of baffles. In the present paper an interaction of chemical kinetics, radiation attenuation, and mixing in isothermal systems is discussed, which may be related to the reported improvement in photoreactor performance. In the course of describing the interaction it is necessary to treat the absence of mixing as well as its presence. Interesting effects are found in both cases. The interaction may in principle be found both in photochemical reactors and in radiation chemical reactors. Both types of reactor will therefore be implied in the use of the term *photoreactor*.

Photochemists have been aware of the interaction for some time. It was evidently first described by Bhagwat and Dhar (*6*) in 1932. These authors showed that two conditions had to be satisfied in order for a mixing effect to exist: (1) the local reaction rate had to depend on a power of the locally absorbed radiation intensity other than unity, and (2) the absorbing reactant layer had to be optically thick. It was shown mathematically for a photoreaction whose rate depended on a power of the absorbed intensity less than one that stirring increased the observed rate of the reaction. The greater the optical density of the reaction mixture, the greater the increase in rate.*

To the two conditions set forth by Bhagwat and Dhar a third must be added, which arises from consideration of reaction mechanism and relative time scales of chemical kinetics and mixing processes, as will be seen below.

Information on reaction mechanism is implicit in the form of the intensity dependence of the reaction rate (*7*). Photoreactions whose rate depends on $(I_a)^{1/n}$, where $n \geq 1$, include chain reactions for which n is the order of the predominant chain-breaking step with respect to chain carrier. If termination occurs primarily by a reaction that is first order with respect to chain carrying radical, $n = 1$ and the first condition for the existence of a mixing effect is not satisfied. If most chains terminate by radical-radical reaction, $n = 2$ and a mixing effect may occur.

The overall rate of a chain reaction is often directly proportional to the concentration of reactive intermediates. In an optically dense system in the absence of mixing or appreciable diffusion, a nonuniform distribution of intermediates is developed as a result of nonuniform ab-

Richard M. Felder is at Princeton University, Princeton, New Jersey.

* While true for the slab geometry considered by Bhagwat and Dhar, this statement is not true in general. For instance, for a certain region of optical density it is not true for the cylinder, as will be evident later.